electronics

Article

Dual-Wavelength Mode-Locked Oscillation with Graphene Nanoplatelet Saturable Absorber in Erbium-Doped Fiber Laser

Ahmad Fauzi Abas [1,*], Kuen Y. Lau [2], Farah D. Muhammad [3], Wazie M. Abdulkawi [1,4], Yahya M. Al-Moliki [1], Mohammed T. Alresheedi [1] and Mohd Adzir Mahdi [5]

[1] Department of Electrical Engineering, College of Engineering, King Saud University, P.O. Box 800, Riyadh 11421, Saudi Arabia
[2] State Key Laboratory of Modern Optical Instrumentation, College of Optical Science and Engineering, Zhejiang University, Hangzhou 310027, China
[3] Department of Physics, Faculty of Science, Universiti Putra Malaysia, Serdang 43400, Selangor, Malaysia
[4] Department of Electrical Engineering, College of Engineering in Wadi Addawasir, Prince Sattam bin Abdulaziz University, Al-Kharj 11991, Saudi Arabia
[5] Wireless and Photonics Networks Research Centre, Faculty of Engineering, Universiti Putra Malaysia, Serdang 43400, Selangor, Malaysia
* Correspondence: aabas@ksu.edu.sa

Abstract: In this work, we demonstrate a dual-wavelength passively mode-locked erbium-doped fiber laser employing graphene nanoplatelet as saturable absorber. The dual-wavelength laser is generated in ~1530 nm and ~1550 nm wavelength regions by splitting the main signal into two separate laser oscillations via a red/blue wavelength division multiplexer. Both the unidirectional and bidirectional dual-wavelength oscillation scheme are investigated, and it is found that the latter is advantageous in providing narrower pulse widths of 890 fs and 980 fs for the respective wavelength region, on top of boosting the pulse energy to the maximum value of 139 pJ and 155 pJ, respectively. It is believed that the bidirectional dual-wavelength oscillation scheme can minimize the overlapping effect between the neighboring pulses that cause pulse distortion as well as signal attenuation compared with unidirectional dual-wavelength oscillation. This work expands the dynamics of cavity structure design for synchronized dual-wavelength mode-locked fiber laser generation.

Keywords: mode-locked oscillation; saturable absorber; graphene nanoplatelet

check for updates

Citation: Abas, A.F.; Lau, K.Y.; Muhammad, F.D.; Abdulkawi, W.M.; Al-Moliki, Y.M.; Alresheedi, M.T.; Mahdi, M.A. Dual-Wavelength Mode-Locked Oscillation with Graphene Nanoplatelet Saturable Absorber in Erbium-Doped Fiber Laser. *Electronics* **2022**, *11*, 2880. https://doi.org/10.3390/electronics11182880

Academic Editor: Ju Han Lee

Received: 3 August 2022
Accepted: 7 September 2022
Published: 12 September 2022

1. Introduction

Compact dual-wavelength mode-locked fiber lasers have attracted great attention due to their wide applications such as fiber optic sensing, wavelength-division-multiplexed communication systems, optical spectroscopy, biomedical imaging and terahertz radiation generation [1–6]. Among various approaches that have been investigated to realize dual-wavelength mode-locked fiber laser, the saturable absorption effect is one of the promising mechanisms for generating pulse operation in dual-wavelength laser system [7–9]. In general, this effect is introduced by materials with nonlinear dependence of their transmittance, which greatly increases with incident optical power, thus enabling the pulse operation to be more energetically efficient and therefore preferable [10].

Concurrently, new kinds of 2D materials keep emerging as new potential saturable absorbers owing to their excellent optical properties such as short recovery time, small bandgap energy, broadband absorption and high compatibility with fiber laser systems. This includes materials from the group of transition metal oxides [11–13], transition metal dichalcogenides [14,15] and topological insulators [16,17]. Undeniably, the advancement of these materials can be traced back to the superiority and versatility of their pioneer, graphene, which is still worthy of investigation to date [18–25]. This is attributed to its desirable properties such as gapless linear dispersion of Dirac-electrons, short recovery time and ultra-broadband absorption [21]. Several forms of graphene include monolayer graphene, graphene oxide, reduced graphene oxide and graphene nanoplatelet. Unlike other forms of graphene, graphene nanoplatelets typically exists in a stack of multiple single layers of graphene [26], which normally have a thickness of between 1–3 nanometers and lateral dimensions ranging from 100 nanometers to 100 microns. This makes graphene nanoplatelets more feasible as saturable absorbers compared with monolayer graphene and graphene oxide since it offers higher possibility to exhibit high modulation depth and low defect density [27].

A challenge in dual-wavelength mode-locking is to select the desired wavelength operation without suppressing or affecting the other. The method of loss management in the laser cavity through macrobending loss utilizing the fiber spooling technique has been introduced in ref. [28]. This technique allows the selection of single- or dual-lasing operations without requiring an external tunable attenuator device integrated into the laser cavity. However, cavity loss controlled by macrobending loss strictly depends on the radius of the fiber spooling. For instance, a small difference in spooling radius of 0.8 cm is already capable to disrupt the dual-lasing operation [28]. Another method of intracavity loss control by tailoring the polarization state to obtain switchable dual-wavelength mode-locked lasers is presented in ref. [29], but the achievable pulse width is limited to picosecond range. On the other hand, a double-ring laser resonator with different types of gain medium in each loop has been proposed for generating dual-wavelength mode-locked lasers that oscillate simultaneously yet can be independently controlled [30], however, at the expense of system complexity with a double pumping scheme. While the knowledge of dual-wavelength mode-locked laser mechanisms and intracavity dynamics are still at the infancy stage and elusive, there is still a need to extend the research to establish alternative systems that can bridge the existing gaps to improve the performance of dual-wavelength mode-locked lasers.

In this work, a dual-wavelength passively mode-locked erbium-doped fiber laser is constructed based on the dual-cavity loop from a single pumping scheme and a mutual mode-locking element incorporating graphene nanoplatelet (GNP) saturable absorber (SA). To form the dual-cavity loop configuration, two red/blue wavelength division multiplexers are used to split and recombine the signals, respectively. At the first stage, the dual-wavelength signals are made to circulate in unidirectional oscillation. The laser emission is observed to occur at two distinct wavelengths of ~1530 nm and ~1550 nm, corresponding to each cavity loop. For comparison purpose, the laser resonator is modified to let both laser emissions oscillate bidirectionally. Interestingly, the bidirectional dual-wavelength oscillation shows better performance in certain aspects, such as producing narrower pulse width and higher pulse energy. The obtained results indicate that the proposed system could be a good alternative for synchronized dual-wavelength mode-locked generation.

2. Characterization of Graphene Nanoplatelets Saturable Absorber

In this work, GNP in powder form is employed, which is produced from expandable graphite (3772, Asbury Carbons, Inc., Asbury, NJ, USA). The detailed synthesis process of the GNP powder is described in ref. [31]. Subsequently, GNP SA is assembled by depositing the GNP powder on a clean FC/PC fiber ferrule, which is then connected to another fiber ferrule to form a sandwiched-type structure. The fabrication procedure of the GNP SA is similar to the one reported in ref. [27]. The prepared GNP SA is then examined using a WITec Raman spectroscopy (Alpha 300R) with ~488 nm excitation wavelength, and the result is shown in Figure 1. The intensity peaks exhibited at Raman shift of approximately 1570 cm^{-1} (G peak) and 2700 cm^{-1} (2D peak) match the specified Raman spectrum peak profiles for graphene [32,33], which indicate that the GNP is successfully deposited on the fiber ferrule. The estimated G/2D intensity ratio of <2 denotes that the deposited GNP is multilayer.

Characterization of the nonlinear optical properties of the GNP SA is carried out based on power-dependent transmission measurement by using an equalized twin detector system. The system consists of an M-fiber MenloSystem pulse fiber laser source connected to a variable optical attenuator and a 50:50 optical coupler to split the pulse laser signal into two equal portions. The pulse laser, which operates at 1560 nm, has a pulse repetition rate of 250 MHz and pulse duration of 117 fs. The nonlinear saturable absorption result is shown in Figure 2, which agrees with the formula in Equation (1) [34];

$$\alpha(I) = \frac{\alpha_0}{1 + \frac{I}{I_{sat}}} + \alpha_{ns}, \quad (1)$$

where $\alpha(I)$ is the intensity-dependent absorption coefficient, I_{sat} is the saturation intensity, α_0 is the modulation depth, I is the peak intensity and α_{ns}, is the nonsaturable absorbance. Based on the curve fitting, the estimated values of α_0 and I_{sat} for the GNP SA are 0.66% and 9.8 MW/cm^2, respectively.

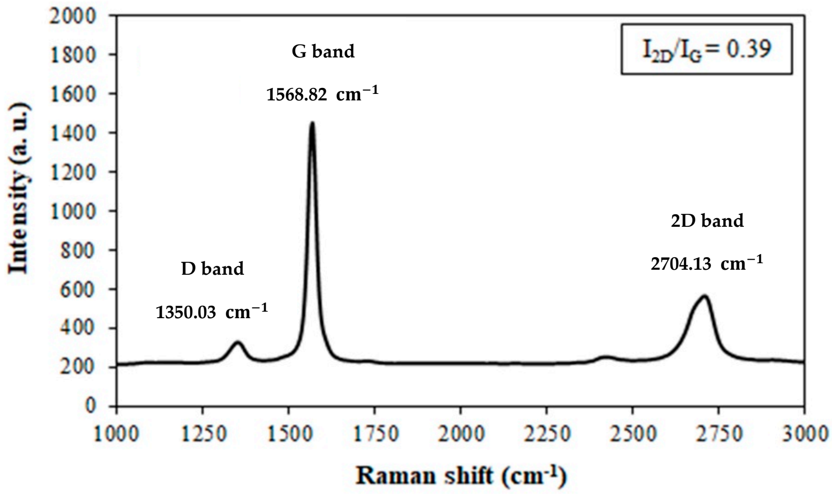

Figure 1. Raman spectrum of the GNP SA deposited on fiber ferrule.

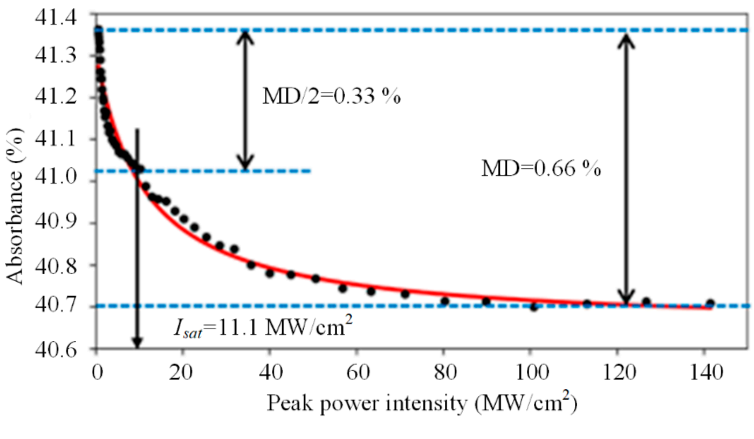

Figure 2. Nonlinear saturable absorbance properties of GNP SA.

3. Experimental Setup

The experimental setup of the dual-wavelength passively mode-locked erbium-doped fiber laser (DWML-EDFL) system is shown in Figure 3, in which the unidirectional and bidirectional signal oscillation in the common branch are, respectively, established to investigate the impact of the propagation directivity on the output pulse performance. The common branch consists of a 4.5 m-length erbium-doped fiber (EDF) gain medium with a signal absorption coefficient of 3.5 dB/m at 1530 nm, which is pumped by a 980 nm laser diode (LD) through a 980/1550 nm wavelength selective coupler (WSC). The GNP SA is placed after the EDF as the mode locking element, and it is then connected to a polarization controller (PC). A red/blue wavelength division multiplexer (R/B WDM-1) is used to split the signal from the PC into two distinct wavelengths, namely $\lambda(-)$ and $\lambda(+)$, which are located at ~1530 nm and ~1555 nm, respectively. The separation efficiency of the R/B WDM is 15.5 and 33.5 dB for 1530 and 1555 nm ports, correspondingly. In the case of unidirectional signal oscillation, as shown in Figure 3a, the oscillating signals are recombined through R/B WDM-2 to be guided back into the common branch. An isolator (ISO) is placed in between the R/B WDM-2 and the 1550 nm port of the WDM to ensure unidirectional signal propagation within the common branch. On the other hand, for the case of bidirectional signal oscillation, the ISO and R/B WDM-2 are replaced with an optical circulator (CIR). This arrangement enables opposite propagation directivity between $\lambda(-)$ and $\lambda(+)$ in the common branch as shown in Figure 3b. Based on the respective oscillation directions, both $\lambda(-)$ and $\lambda(+)$ signals are channeled to optical couplers, denoted as OC-1 and OC-2, respectively, to extract 30% of each signal for further analysis. The remaining signals of both $\lambda(-)$ and $\lambda(+)$ are then channeled through the 70% port of the respective OC-1 and OC-2.

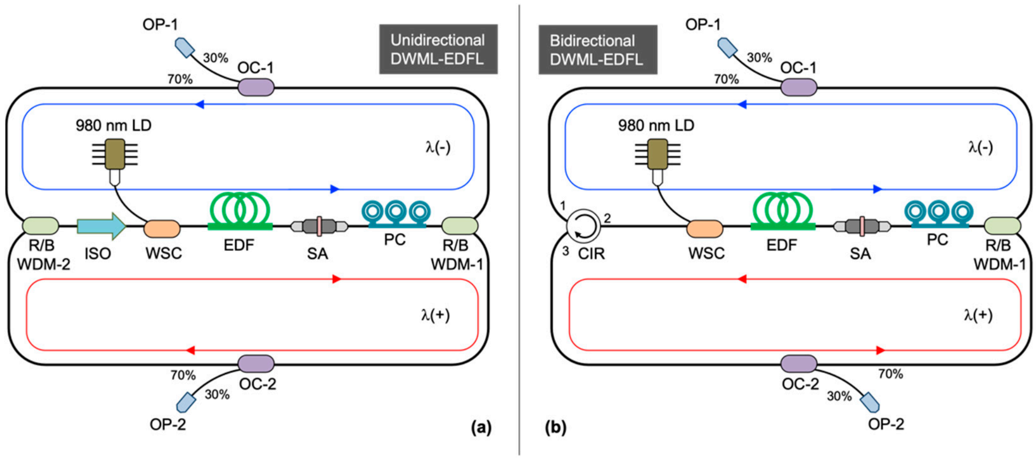

Figure 3. Experimental setup of (**a**) unidirectional and (**b**) bidirectional DWML-EDFL.

4. Results and Discussion

Figure 4a,b shows the evolution of the mode-locked output spectrum against pump power for unidirectional DWML-EDFL and bidirectional DWML-EDFL, respectively. This measurement is taken by using an optical spectrum analyzer (Yokogawa AQ6370B, Tokyo, Japan) with 0.02 nm resolution bandwidth. After optimizing the PC state, the mode-locked operation is achieved at the pump power threshold of 41.3 mW and 38.4 mW for unidirectional and bidirectional DWML-EDFL, respectively. At the maximum pump power of 105.2 mW, the central wavelength of $\lambda(-)$ signals are ~1533 nm for both unidirectional and bidirectional DWML-EDFL, with 3 dB spectral bandwidth of ~3.0 nm. On the other hand, for $\lambda(+)$ signals, the central wavelength are ~1557 nm and 1555 nm for unidirectional and bidirectional DWML-EDFL, respectively, with their respective 3 dB spectral bandwidths of 2.4 nm and 3.2 nm. By taking the dispersion coefficient (β_2) values of -22, -7 and 23 ps^2/km for SMF-28, Hi-1060 SMF and EDF, respectively, the estimated net group velocity dispersion (GVD) for all the cavity loops are calculated within the range of -0.3215 to -0.2797 ps^2, which falls in the anomalous dispersion regime. The existence of Kelly sidebands in the mode-locked spectrum confirms the soliton operation of a pulse laser.

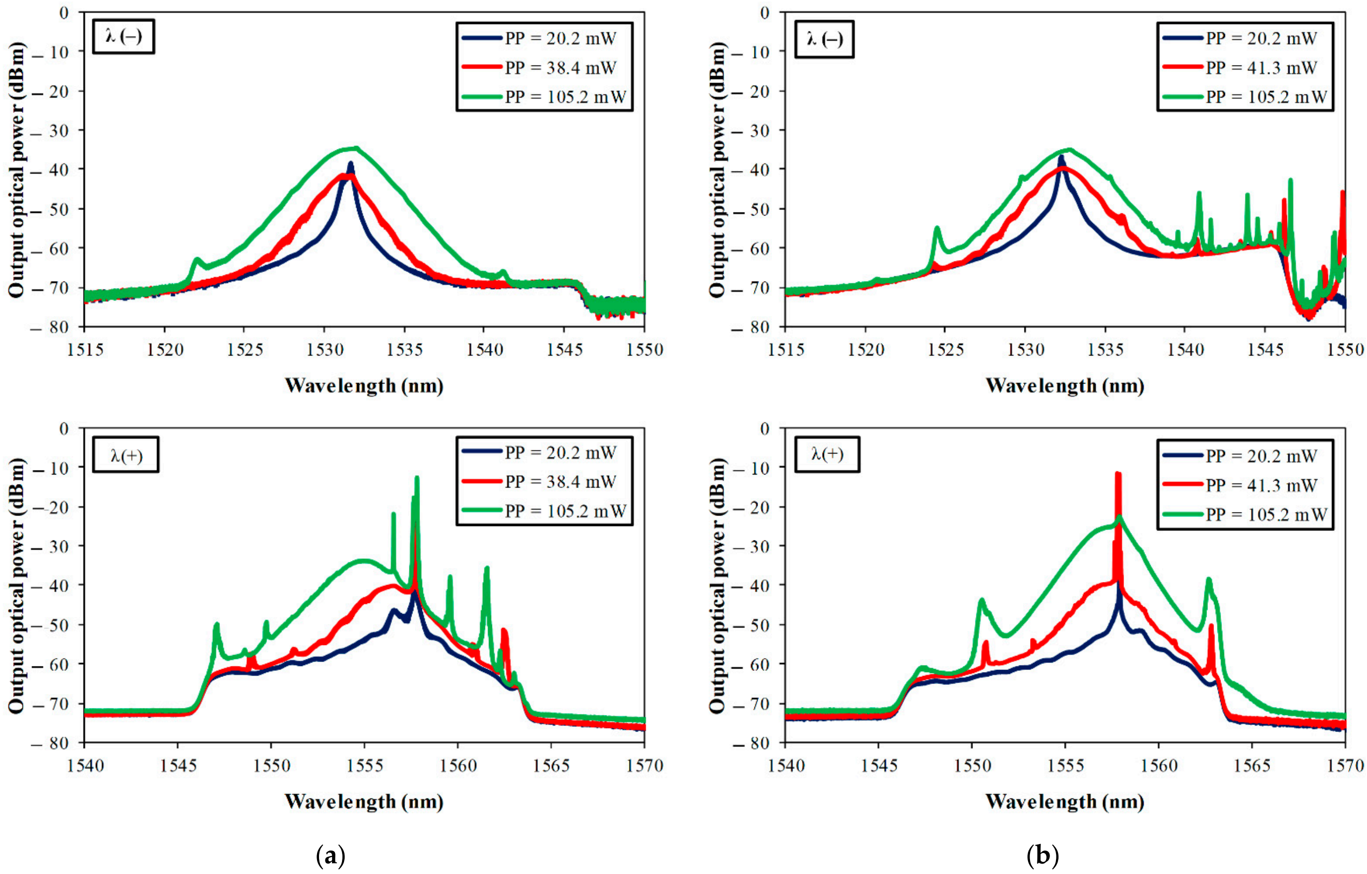

Figure 4. Output spectrum against pump power for (**a**) unidirectional DWML-EDFL and (**b**) bidirectional DWML-EDFL.

The autocorrelation trace of the mode-locked pulse is measured by using an autocorrelator (Alnair HAC-200). By assuming the sech2 pulse shape fitting, the full width at half maximum (FWHM) pulse duration is 900 fs for λ(−) signal and 1020 fs for λ(+) signal in the unidirectional DWML-EDFL, as shown in Figure 5a. On the other hand, for the bidirectional DWML-EDFL, the narrower pulse widths of 890 fs and 980 fs are obtained for λ(−) and λ(+), respectively, as shown in Figure 5b.

The mode-locked pulse train for each cavity loop is measured using an oscilloscope (Tektronix TDS 3012C) together with a 5 GHz In GaAs-biased photodetector (Thorlabs, DET08CFC, Newton, MA, USA). The results are shown in Figure 6a,b, corresponding to unidirectional and bidirectional DWML-EDFL, respectively. Since the total cavity length of all the cavity loops is almost similar, about 17 m, the pulse repetition rate for each cavity loop does not vary much between one another, with the values ranging from 9.22 MHz to 9.29 MHz. The evenly spaced pulse interval between the consecutive pulses validates the good stability of the pulse output.

Figure 7a,b shows the radio frequency (RF) spectrum of the mode-locked output at fundamental frequency peak for unidirectional and bidirectional DWML-EDFL, respectively, which are measured at the RF span of 1 MHz and resolution bandwidth of 30 kHz. For λ(−) and λ(+) signals in unidirectional DWML-EDFL, the peak-to-pedestal extinction ratios (PER) are 40.78 dB and 39.53 dB, respectively. On the other hand, for λ(−) and λ(+) signals in bidirectional DWML-EDFL, the measured PERs are 42.92 dB and 37.70 dB, respectively.

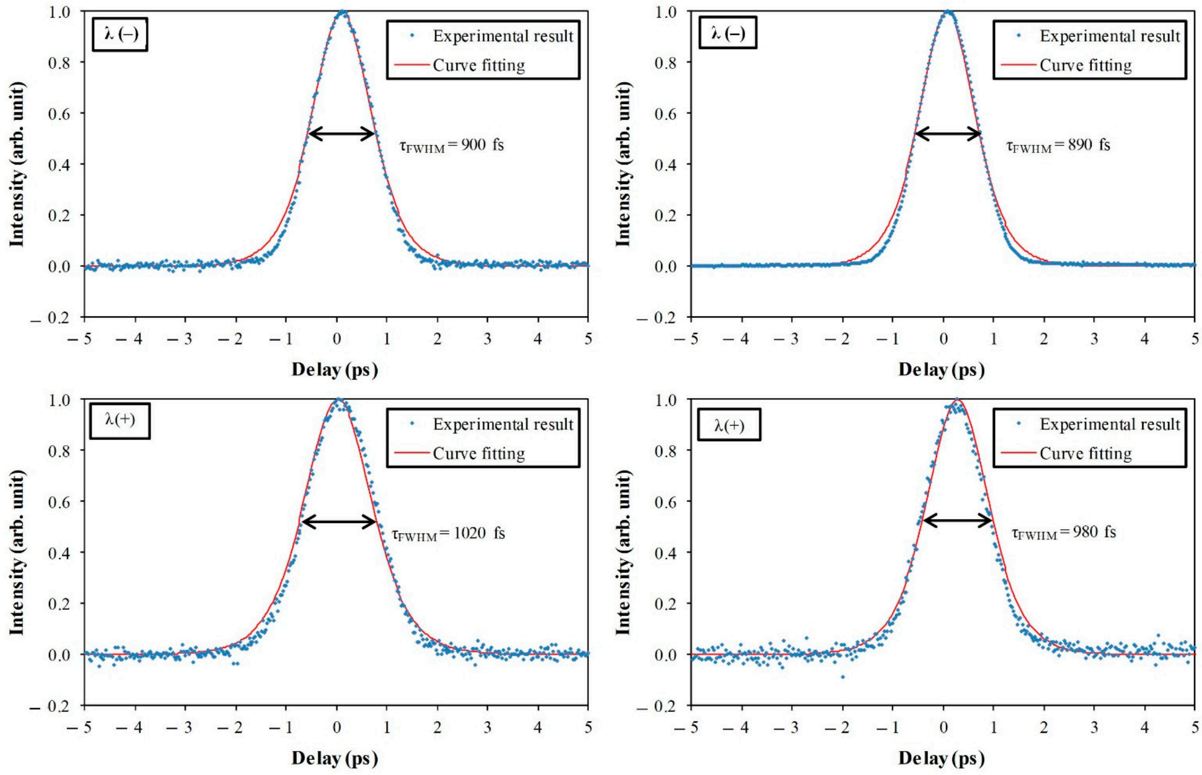

(**a**) (**b**)

Figure 5. Autocorrelation trace for (**a**) unidirectional DWML-EDFL and (**b**) bidirectional DWML-EDFL at maximum pump power of 105.2 mW.

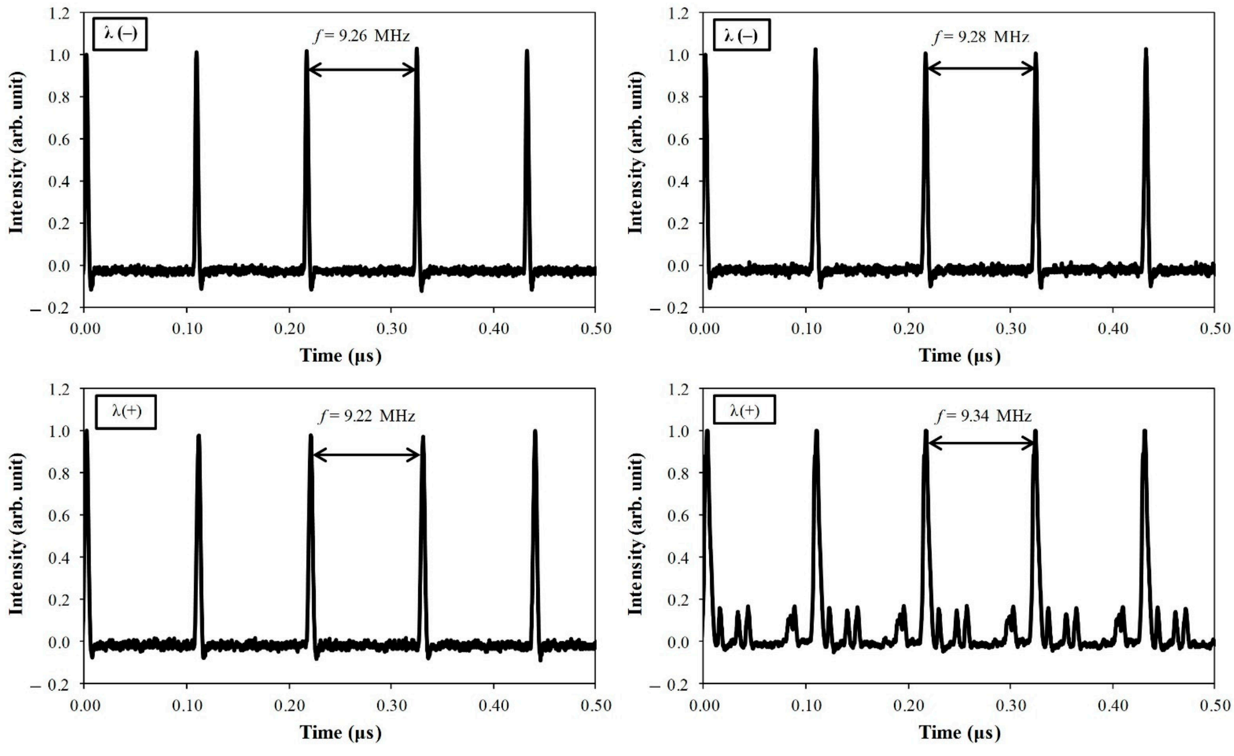

(**a**) (**b**)

Figure 6. Pulse train for (**a**) unidirectional DWML-EDFL and (**b**) bidirectional DWML-EDFL.

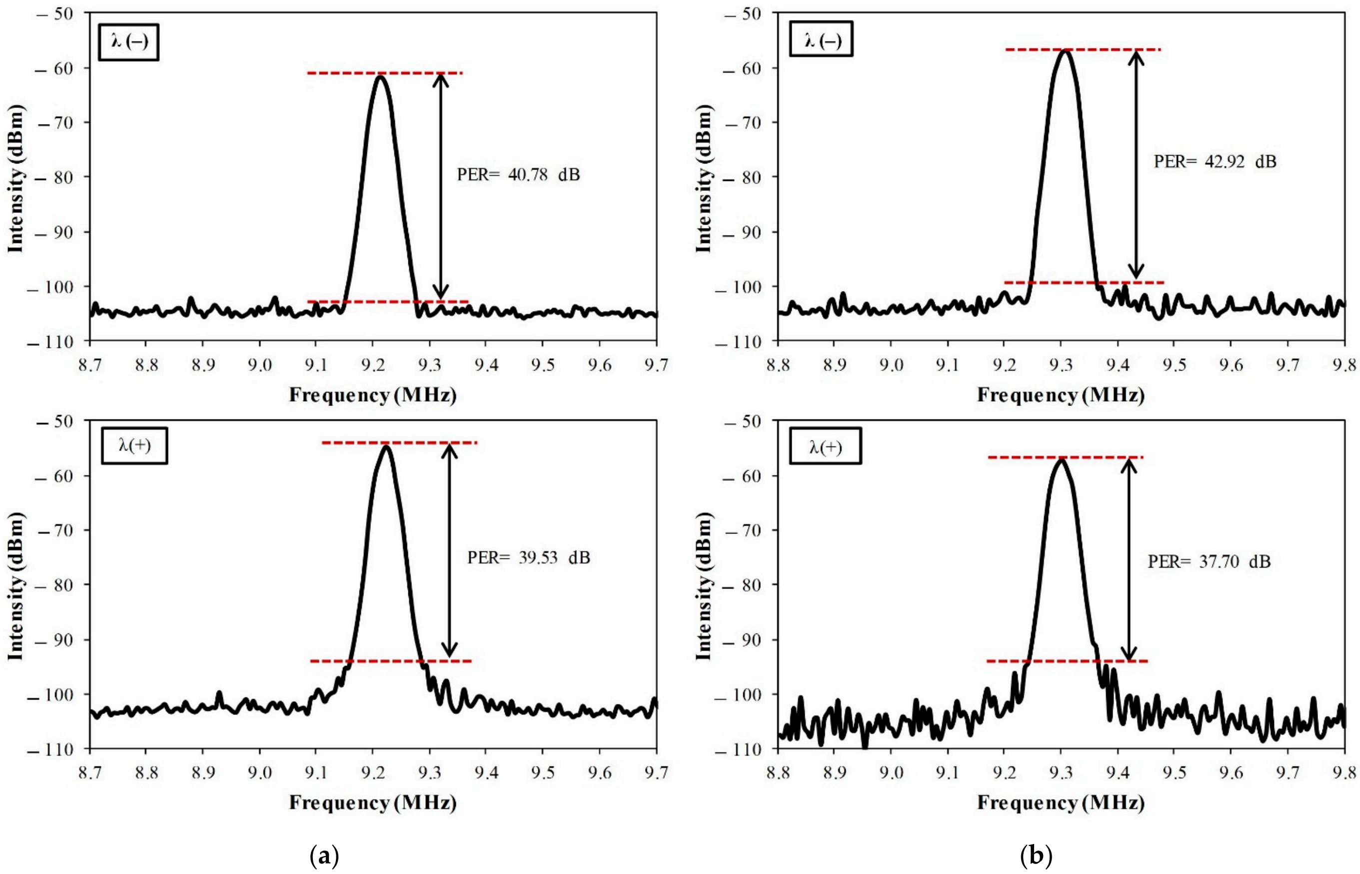

Figure 7. RF spectrum at fundamental frequency peak for (**a**) unidirectional DWML-EDFL and (**b**) bidirectional DWML-EDFL.

The results of average output power and pulse energy evolution versus pump power for unidirectional and bidirectional DWML-EDFL are shown in Figure 8a,b, respectively. Based on the graph of output power development, all λ(−) and λ(+) signals in both unidirectional and bidirectional DWML-EDFL have a similar lasing threshold of about 20 mW. It can also be seen that the average output power increases almost linearly against the pump power for all the cavity loops. This linear increment behavior is also observed for the case of pulse energy. The maximum average output power, power slope efficiencies, mode-locking threshold and maximum pulse energy for the respective cavity loop are tabulated in Table 1. It is worth noting that the mode-locking threshold for both λ(−) and λ(+) signals in bidirectional DWML-EDFL is lower than that of the unidirectional DWML-EDFL, with the respective values of 38 mW for bidirectional and 41 mW for unidirectional DWML-EDFL. On top of that, narrower pulse widths of 890 fs and 980 fs are obtained for λ(−) and λ(+), respectively, in bidirectional DWML-EDFL compared with those of unidirectional DWML-EDFL, with the pulse width value of 900 fs for λ(−) signal and 1020 fs for λ(+) signal. In addition, the maximum average output power and pulse energy in the bidirectional DWML-EDFL are observed to be higher than those of the pertinent signals in the unidirectional DWML-EDFL. Although the cavity loss for the bidirectional DWML-EDFL is marginally lower than its counterpart, the amplification condition plays significant role for these two laser schemes. For the unidirectional case, both laser signals propagate into the EDF at the same entry point. Both signals are amplified together towards the other end of the EDF. Under this condition, the absorption of the 980 nm pump light is rapid as a result of faster pump depletion. The localized population inversion at the output end of EDF (just before SA) is very low, the excited electrons are inadequate to cater to huge numbers of incoming photons. On the other hand, for the bidirectional laser cavity, the laser signals propagate into the EDF in the opposite direction. The pump depletion is more balanced since the localized number of photons is almost similar throughout the EDF. As a result, the variation of localized population inversion is also minimal, which leads to better lasing performances as compared with the unidirectional laser cavity.

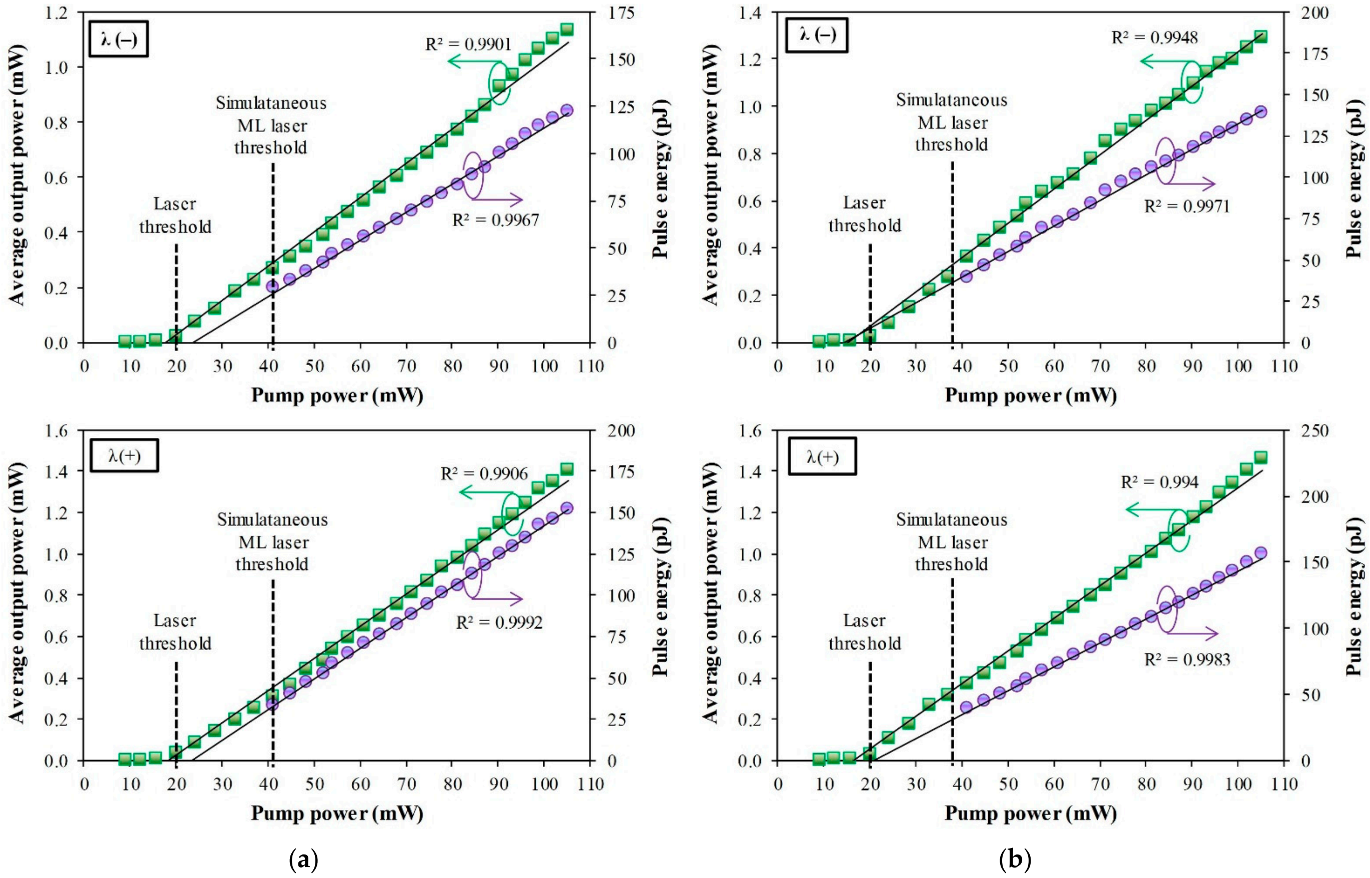

Figure 8. Average output power and pulse energy against pump power for (**a**) unidirectional DWML-EDFL and (**b**) bidirectional DWML-EDFL.

Table 1. Comparison of output pulse performance for unidirectional and bidirectional DWML-EDFL.

Laser Cavity Configuration	Unidirectional DWML-EDFL		Bidirectional DWML-EDFL	
Optical loops	$\lambda(-)$	$\lambda(+)$	$\lambda(-)$	$\lambda(+)$
Maximum output power (mW)	1.13	1.4	1.29	1.46
Slope efficiencies (%)	1.35	1.71	1.45	1.7
Mode-locking threshold (mW)	41	41	38	38
Maximum pulse energy (pJ)	122	152	139	155
3 dB bandwidth (nm)	3.0	2.4	3.0	3.2
Pulse width (fs)	900	1020	890	980
Repetition rate (MHz)	9.26	9.22	9.29	9.35
PER (dB)	40.78	39.53	42.92	37.70

5. Conclusions

We investigated a dual-wavelength passively mode-locked erbium-doped fiber laser based on the dual-cavity loop from a single pumping scheme and a mutual mode-locking element incorporating graphene nanoplatelet saturable absorber. The fiber laser configuration is initially designed to allow unidirectional signal oscillation through a common gain medium and saturable absorber. Mode-locked laser outputs are successfully generated at two different wavelengths of ~1530 nm and ~1550 nm, respectively. For comparison purposes, the cavity configuration is then modified to divert the signal direction from unidirectional to bidirectional oscillation. Results show that the bidirectional dual-wavelength oscillation scheme exhibits better performance over the unidirectional scheme in certain aspects, such as in terms of providing shorter pulse width, higher pulse energy, lower mode-locked threshold and higher maximum output power, without compromising the pulse stability. The bidirectional dual-wavelength oscillation scheme is capable of delivering pulse durations of 890 fs and 980 fs as well as maximum pulse energies of 139 pJ and 155 pJ for the respective λ(−) and λ(+) signals. This work also validates the cavity structure design to produce dual-femtosecond laser outputs with minimal usage of optical components including saturable absorber.

Author Contributions: Conceptualization, A.F.A., K.Y.L. and M.A.M.; methodology, A.F.A., K.Y.L., M.T.A. and M.A.M.; software, K.Y.L.; validation, A.F.A., K.Y.L. and M.A.M.; formal analysis, A.F.A., K.Y.L., W.M.A., Y.M.A.-M., M.T.A., F.D.M. and M.A.M.; investigation, A.F.A., K.Y.L., W.M.A., Y.M.A.-M., M.T.A., F.D.M. and M.A.M.; resources, A.F.A., M.T.A. and M.A.M.; data curation, K.Y.L.; writing—original draft preparation, K.Y.L. and W.M.A.; writing—review and editing, A.F.A., K.Y.L., W.M.A., Y.M.A.-M., M.T.A., F.D.M. and M.A.M.; visualization, A.F.A., K.Y.L., M.T.A. and M.A.M.; supervision, A.F.A., M.T.A. and M.A.M.; project administration, A.F.A., M.T.A. and M.A.M.; funding acquisition, A.F.A. and M.T.A. All authors have read and agreed to the published version of the manuscript.

Funding: National Plan for Science, Technology and Innovation (MAARIFAH), King Abdulaziz City for Science and Technology, Kingdom of Saudi Arabia, Award Number 3-17-09-001-0007.

Acknowledgments: This project was funded by the National Plan for Science, Technology and Innovation (MAARIFAH), King Abdulaziz City for Science and Technology, Kingdom of Saudi Arabia, Award Number 3-17-09-001-0007.

Conflicts of Interest: The authors declare no conflict of interest.

References

1. Tang, Y.; Li, F.; Yu, X. Dual-wavelength harmonic mode-locked dissipative soliton resonance of Yb fiber laser. *Opt. Laser Technol.* **2022**, *152*, 108147. [CrossRef]
2. Liu, T.; Yan, M.; Guo, Z.; Zeng, H. Mechanisms of Dual-Wavelength Mode-Locking in Fiber Lasers. 2022. Available online: http://dx.doi.org/10.2139/ssrn.4008868 (accessed on 20 July 2022).
3. Long, J.; Gao, Y.; Lin, W.; Wu, J.; Lin, X.; Hong, W.; Cui, H.; Luo, Z.; Xu, W.; Luo, A.-P. Switchable and spacing tunable dual-wavelength spatiotemporal mode-locked fiber laser. *Opt. Lett.* **2021**, *46*, 588–591. [CrossRef] [PubMed]
4. Wang, Z.; Liu, C.; Su, X.; Wang, Y.; Xie, Y.; Gao, F.; Kumar, S.; Zhang, B. Dual-wavelength mode-locked laser based on optimization of erbium-doped fiber length. *Optik* **2021**, *251*, 168370. [CrossRef]
5. Armas-Rivera, I.; Rodriguez-Morales, L.A.; Durán-Sánchez, M.; Ibarra-Escamilla, B. Dual-wavelength mode-locked Er-doped fiber laser in a spectral filter free cavity. *Opt. Laser Technol.* **2021**, *142*, 107222. [CrossRef]
6. Luo, X.; Tuan, T.; Saini, T.; Nguyen, H.; Suzuki, T.; Ohishi, Y. Switchable dual-wavelength mode-locked fiber laser using Saganc loop mirror. *Opt. Commun.* **2020**, *463*, 125457. [CrossRef]
7. Li, S.; Yin, Y.; Ran, G.; Ouyang, Q.; Chen, Y.; Tokurakawa, M.; Sulaiman, E.L.; Harun, W.; Wang, P. Dual-wavelength mode-locked erbium-doped fiber laser based on tin disulfide thin film as saturable absorber. *J. Appl. Phys.* **2019**, *125*, 243104. [CrossRef]
8. Lau, K.Y.; Zulkifli, M.Z. 1.56 μm and 1.93 μm synchronized mode-locked fiber laser with graphene saturable absorber. *Infrared Phys. Technol.* **2021**, *112*, 103606. [CrossRef]
9. Lau, K.Y.; Abu Bakar, M.H.; Muhammad, F.D.; Latif, A.A.; Omar, M.F.; Yusoff, Z.; Mahdi, M.A. Dual-wavelength, mode-locked erbium-doped fiber laser employing a graphene/polymethyl-methacrylate saturable absorber. *Opt. Express* **2018**, *14*, 12790–12800. [CrossRef]
10. Kobtsev, S.M. Artificial saturable absorbers for ultrafast fibre lasers. *Opt. Fiber Technol.* **2022**, *68*, 102764.
11. Xu, D.; Zhang, H.; Peng, J.; Chen, J.; Yang, X.; Li, D.; Li, Z.; Zheng, Y. Passively mode-locked ytterbium-doped fiber laser based on Fe_3O_4 nanosheets saturable absorber. *Photonics* **2022**, *9*, 306. [CrossRef]
12. Dong, L.; Chu, H.; Li, Y.; Zhao, S.; Li, D. Third-order nonlinear optical responses of CuO nanosheets for ultrafast pulse generation. *J. Mater.* **2022**, *8*, 2–511. [CrossRef]
13. Hou, R.; Li, H.; Diao, M.; Sun, Y.; Liang, Z.; Yu, Z.; Huang, Z.; Zhang, C. Fast electrochemical activation of the broadband saturable absorption of tungsten oxide nanoporous film. *Nano Res.* **2022**, *15*, 326–332. [CrossRef]

14. Ahmad, H.; Hidayah, N.; Yusoff, N.; Zharif, M.; Aisyah, S.; Faizal, M.; Bayang, L.; Wang, Y.; Wang, S.; Sahu, J. Passively Q-switched 1.3 µm bismuth doped-fiber laser based on transition metal dichalcogenides saturable absorbers. *Opt. Fiber Technol.* **2022**, *69*, 102851. [CrossRef]
15. He, J.; Lu, H.; Tao, L.; Zhao, Y.; Zheng, Z.; Zhou, B. Novel two-dimensional semi-metallic NiTe2 based saturable absorber for ultrafast mode-locked fiber laser. *Infrared Phys. Technol.* **2022**, *123*, 104195. [CrossRef]
16. Haris, H.; Batumalay, M.; Tan, S.J.; Markom, A.M.; Muhammad, A.R.; Harun, S.W.; Megat Hasnan, M.M.I.; Saad, I. Mode-Locked YDFL Using Topological Insulator Bismuth Selenide Nanosheets as the Saturable Absorber. *Crystals* **2022**, *12*, 489. [CrossRef]
17. Zhang, X.; Xing, X.; Li, J.; Peng, X.; Qiao, L.; Liu, Y.; Xiong, X.; Han, J.; Liu, W.; Xiao, W.; et al. Controllable epitaxy of quasi-one-dimensional topological insulator α-Bi4Br4 for the application of saturable absorber. *Appl. Phys. Lett.* **2022**, *120*, 093103. [CrossRef]
18. Ai, F.; Li, X.; Qian, J. Dual-wavelength mode-locked fiber laser based on graphene materials. *Eur. Phys. J. Spec. Top.* **2022**, *231*, 643–649. [CrossRef]
19. Hua, K.; Wang, D.N.; Chen, Q. Passively mode-locked fiber laser based on graphene covered single-mode fiber with inner short waveguides. *Opt. Commun.* **2022**, *505*, 127520. [CrossRef]
20. Li, X.; Wang, D.N.; Hua, K.; Chen, Q.; Ge, Y.; Xia, Q.K. Saturable absorber based on graphene for a hybrid passive mode-locked erbium-doped fiber laser. *Opt. Fiber Technol.* **2022**, *70*, 102867. [CrossRef]
21. Abas, A.F.; Lau, K.Y.; Abdulkawi, W.M.; Alresheedi, M.T.; Muhammad, F.D.; Mahdi, M.A. Dispersion management and pulse characterization of graphene-based soliton mode-locked fiber lasers. *Appl. Sci.* **2022**, *12*, 3288. [CrossRef]
22. Yap, Y.; Chong, W.; Razgaleh, S.A.; Huang, N.; Ong, C.; Ahmad, H. Performance of Q-switched fiber laser using optically deposited reduced graphene oxide as saturable absorber. *Fiber Integr. Opt.* **2022**, *41*, 26–40. [CrossRef]
23. Ponarina, M.; Okhrimchuk, A.; Alagashev, G.; Orlova, G.; Dolmatov, T.; Rybin, M.; Obraztsova, E.; Bukin, V.; Obraztsov, P. Wavelength-switchable 9.5 GHz graphene mode-locked waveguide laser. *Appl. Phys. Express* **2021**, *14*, 072001. [CrossRef]
24. Hua, K.; Wang, D.N. Coupling scheme for graphene saturable absorber in a linear cavity mode-locked fiber laser. *Opt. Lett.* **2021**, *46*, 17–4362. [CrossRef] [PubMed]
25. Peng, X.; Yan, Y. Graphene saturable absorbers applications in fiber lasers. *J. Eur. Opt. Soc. Rapid Publ.* **2021**, *17*, 16.
26. Wang, F.; Drzal, L.T.; Qin, Y.; Huang, Z. Mechanical properties and thermal conductivity of graphene nanoplatelet/epoxy composites. *J. Mater. Sci.* **2015**, *50*, 1082–1093. [CrossRef]
27. Lau, K.Y.; Zainol Abidin, N.H.; Abu Bakar, M.H.; Latif, A.A.; Muhammad, F.D.; Huang, N.M.; Omar, M.F.; Mahdi, M.A. Passively mode-locked ultrashort pulse fiber laser incorporating multi-layered graphene nanoplatelets saturable absorber. *J. Phys. Commun.* **2018**, *2*, 075005. [CrossRef]
28. Latif, A.A.; Mohamad, H.; Abu Bakar, M.H.; Muhammad, F.D.; Mahdi, M.A. Carbon nanotube-based mode-locked wavelength-switchable fiber laser via net gain cross section alteration. *Laser Phys.* **2016**, *26*, 025106. [CrossRef]
29. Yang, H.R. Switchable dual-wavelength fiber laser mode-locked by monolayer graphene on D-shaped fiber. *J. Mod. Opt.* **2015**, *62*, 1363–1367. [CrossRef]
30. Sotor, J.; Sobon, G.; Tarka, J.; Pasternak, I.; Krajewska, A.; Strupinski, W.; Abramski, K. Passive synchronization of erbium and thulium doped fiber mode-locked lasers enhanced by common graphene saturable absorber. *Opt. Express* **2014**, *22*, 5536–5543. [CrossRef]
31. Hamra, A.A.B.; Lim, H.N.; Chee, W.K.; Huang, N.M. Electro-exfoliating graphene from graphite for direct fabrication of supercapacitor. *Appl. Surf. Sci.* **2016**, *360*, 213–223. [CrossRef]
32. Ferrari, A.C.; Meyer, J.C.; Scardaci, V.; Casiraghi, C.; Lazzeri, M.; Mauri, F.; Piscanec, S.; Jiang, D.; Novoselov, K.S.; Geim, A.K. Raman spectrum of graphene and graphene layers. *Phys. Rev. Lett.* **2006**, *98*, 187401. [CrossRef] [PubMed]
33. Graf, D.; Molitor, F.; Ensslin, K.; Stampfer, C.; Jungen, A.; Hierold, C.; Wirtz, L. Spatially resolved Raman spectroscopy of single-and few-layer graphene. *Nano Lett.* **2007**, *7*, 238–242. [CrossRef] [PubMed]
34. Garmire, E. Resonant optical nonlinearities in semiconductors. *IEEE J. Sel. Quantum Electron.* **2000**, *6*, 1094–1110. [CrossRef]